Report Documentation Page

1. REPORT DATE **29 MAY 2009**	2. REPORT TYPE	3. DATES COVERED **00-00-2009 to 00-00-2009**

4. TITLE AND SUBTITLE **Reliability estimates for flawed mortar projectile bodies**	5a. CONTRACT NUMBER
	5b. GRANT NUMBER
	5c. PROGRAM ELEMENT NUMBER
6. AUTHOR(S)	5d. PROJECT NUMBER
	5e. TASK NUMBER
	5f. WORK UNIT NUMBER

7. PERFORMING ORGANIZATION NAME(S) AND ADDRESS(ES) **US Army Armament Research Development and Engineering Center,AMSRD-AAR-MEF-E,Analysis and Evaluation Division,Picatinny Arsenal,NJ,07806-5000**	8. PERFORMING ORGANIZATION REPORT NUMBER

9. SPONSORING/MONITORING AGENCY NAME(S) AND ADDRESS(ES)	10. SPONSOR/MONITOR'S ACRONYM(S)
	11. SPONSOR/MONITOR'S REPORT NUMBER(S)

12. DISTRIBUTION/AVAILABILITY STATEMENT
Approved for public release; distribution unlimited

13. SUPPLEMENTARY NOTES

14. ABSTRACT
The Army routinely screens mortar projectiles for defects in safety-critical parts. In 2003, several lots of mortar projectiles had a relatively high defect rate, 0.24%. Before releasing the projectiles, the Army reevaluated the chance of a safety-critical failure. Limit state functions and Monte Carlo simulations were used to estimate reliability. Measured distributions of wall thickness, defect rate, material strength, and applied loads were used with calculated stresses to estimate the probability of failure. The results predicted less than one failure in one million firings. As of 2008, the mortar projectiles have been used without any safety-critical incident.

15. SUBJECT TERMS

16. SECURITY CLASSIFICATION OF:			17. LIMITATION OF ABSTRACT	18. NUMBER OF PAGES	19a. NAME OF RESPONSIBLE PERSON
a. REPORT **unclassified**	b. ABSTRACT **unclassified**	c. THIS PAGE **unclassified**	**Same as Report (SAR)**	**8**	

Reliability estimates for flawed mortar projectile bodies

J.A. Cordes *, J. Thomas [1], R.S. Wong [2], D. Carlucci [3]

US Army ARDEC, AMSRD-AAR-MEF-E, Analysis and Evaluation Division, Fuze and Precision Armaments Technology Directorate,
US Army Armament Research Development and Engineering Center, Picatinny Arsenal, NJ 07806-5000, USA

ARTICLE INFO

ABSTRACT

The Army routinely screens mortar projectiles for defects in safety-critical parts. In 2003, several lots of mortar projectiles had a relatively high defect rate, 0.24%. Before releasing the projectiles, the Army reevaluated the chance of a safety-critical failure. Limit state functions and Monte Carlo simulations were used to estimate reliability. Measured distributions of wall thickness, defect rate, material strength, and applied loads were used with calculated stresses to estimate the probability of failure. The results predicted less than one failure in one million firings. As of 2008, the mortar projectiles have been used without any safety-critical incident.

Published by Elsevier Ltd.

1. Introduction

The Army routinely screens mortar bodies for manufacturing defects in critical areas. In 2003, as part of the Army's normal inspection procedure, a small percentage of defects were found in 60-mm mortar bodies, Fig. 1. The drawing specifies a wall thickness between 0.34 and 0.42 cm. The minimum wall thickness in non-conforming shells was 0.24 cm. In response to the finding, the Army screened the suspect mortar bodies at 100% rate by manual gaging the wall thickness. Structural and reliability analyses were completed to:

1 Estimate probability of yielding
2 Estimate the probability of a mortar projectile failure in a gun tube, a safety-critical event

3 Determine if the minimum wall thickness on the drawing was adequate

The probability of a failure in a gun tube was estimated to be less than 1E−8 and acceptable. A number of improvements in the manufacturing and inspection process were also made. This paper describes the structural and reliability study on the 60-mm mortar bodies.

2. Background

2.1. Limit state functions

Limit state functions provide a way to predict reliability as a function of physical equations and random variables. Generally, limit state functions take the form $g(X1, X2,) < $ constant. The variations in the limit state functions provide a means to quantify the probability of failure.

As examples, Heitzer and Staat [1] tied a limit state function to a finite element analysis for in-elastic structural analysis. NASA

* Corresponding author. Tel.: +1 973 724 9146; fax: +1 973 724 2417.
E-mail address: jennifer.cordes@us.army.mil (J.A. Cordes).
[1] Tel.: +1 973 724 5367.
[2] Tel.: +1 973 724 2486.
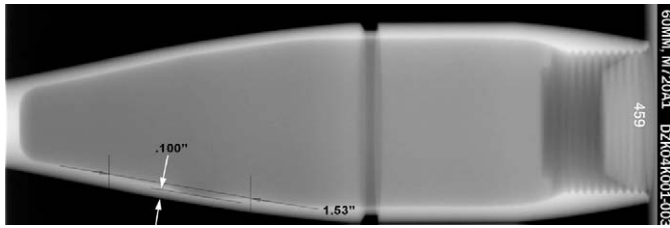[3] Tel.: +1 973 724 4638.

Fig. 1. Screened shell body with anomaly, 60 mm mortar.

scientists are using limit state functions for optimal wing design by combining aerodynamics, computational fluid mechanics, and finite element analysis [2–5]. Shah and Korovaichuk [6] used limit state functions to evaluate fasteners for space structures. Moglia et al. [7] evaluated the probability of a piping system failure using limit state functions. The Army used limit state functions to estimate the likelihood of tolerance stack-up failures in fuzes [8,9].

3. Statistical method

3.1. General approach

In this study, limit state functions were used to compare calculated stresses to material strengths. Reliability predictions were based on limit state functions, finite element results, statistical data, and Monte Carlo simulations. Several limit state functions were considered:

$$G1 = \text{strength-stress\_function} \qquad (1)$$

$$G2 = \text{elongation-stress\_function} \qquad (2)$$

$G1$ is the probability that stress exceeds material strength. Yield strength and ultimate tensile strength were evaluated separately. $G2$ is the probability that strain exceeds material elongation. The probability of failure is the probability that either $G1$ or $G2$ is less than zero.

Two commercially available software packages were used for analysis. DistributionProbe [10] was used determine the best statistical distribution to represent a list of strength and elongation values. The software package included 15 statistical distributions: beta, double exponential, exponential, gamma, Gumbel, Logistic, lognormal, Maxwell, normal, Pareto, Rayleigh, Type I smallest, Type II largest, uniform, and three-parameter Weibull. Three goodness-of-fit tests are available: Anderson–Darling Test, Cramer–von Mises test, and Kolmogorov–Smimov (K–S). The K–S test was based on the largest vertical distance between the empirical distribution and the probability distribution. The user inserted data points and chose a goodness-of-fit criterion. For this study, the K–S test was chosen. DistributionProbe checked the fit of the empirical data against the 15 probability distributions, ranked the distributions based on goodness-of-fit, and provided the statistical parameters for each distribution. The best distribution to represent the data was than used in the Unipass [11] software package to determine probability of failure.

The Unipass [11] package was used to predict the probability that the limit state functions were less than zero, failure. Unipass includes three methods for predicting probability of failure: 1st-order method, 2nd-order method, and Monte Carlo simulation. For this analysis, 1E6 Monte Carlo simulations were used. The 1st- and 2nd-order methods require fewer simulations to predict probability. Unipass input included random variables and limit state functions. Statistical distributions from the DistributionProbe package were used to model yield strength, ultimate tensile strength, and material elongation. A uniform distribution was used to account for geometry variations. The variation in pressure loads in the gun tube was obtained from experiments and known to be close to normal distributions.

For completeness, other modes of structural failure were ruled unlikely. Structures can fail one of three ways: yielding, buckling, or unstable crack growth [12]. The limit state functions G1 and G2 provide failure probability associated with yield failure. Finite element analysis was used to estimate the critical buckling load. The critical buckling force exceeded the 3-sigma compression load by a factor of 7 making buckling unlikely. Finite element analysis of the flawed mortar showed the stress at the flaw edges to be in compression. Since cracks do not grow when the crack tip stress is compressive, this failure mode was also ruled unlikely.

3.2. Strength and elongation functions

The mortar bodies are made of HF-1 steel. HF-1 steel was developed for the Army based on fragmentation requirements [13]. The mortar drawing called for a minimum yield strength of 553 MPa at 2% offset and a minimum elongation of 7%. There is no criterion for ultimate tensile strength for this particular mortar shell.

Limit state functions $G1$ and $G2$ used the material strengths and elongations. This empirical data were gathered from a well-established inspection method. The Army retains inspection reports for each heat treat lot. No field failures have been reported for lots that pass its inspection criteria.

The standard inspection procedure is as follows. For each heat treat lot, material hardness is tested at two locations in mortar bodies. (Hardness is an inexpensive, non-destructive test that correlates loosely with material strength). The projectiles with the highest and lowest hardness were chosen for destructive strength and elongation tests. For each projectile body, two tensile specimens were taken from the forward region and two specimens were taken from the rear taper. Roughly half the data are shown in Table 1. Averages and standard deviations differed slightly between locations and hardness groups. All yield strengths met or exceeded drawing requirements. The minimum elongation from tests, 9%, also exceeded the material requirements stated on the drawings.

For this study, data from 12 lots of heat-treated HF-1 steel was used to determine a statistical distribution. Lots were provided by others, not chosen based on statistical considerations. DistributionProbe [10] was used to determine the statistical distribution for the empirical data points. For the yield strength data, Type I largest Gumble provided the best fit for the three goodness-of-fit tests in DistributionProbe, Fig. 2. The correlation for Gumble using the Kolmogorov–Smirnov (K–S) goodness-of-fit test was 97%. Comparing, the goodness-of-fit for a Weibull and lognormal distribution were 62% and 28%, respectively. When the high-hardness and low-hardness data were evaluated separately, results were similar to the entire population.

Data points from the same 12 lots were also used to find a statistical distribution for elongation data. Using the K–S goodness-of-fit criteria, the best fit was to a Rayleigh distribution at 54%. The elongation distribution is shown in Fig. 3.

The ultimate tensile strength was difficult to determine for the 60-mm mortar shells. It was not tested, not specified on the drawing, not included in the material specification, and not given in the usual references for material properties [14]. The Army metallurgist at Picatinny Arsenal provided measured ultimate tensile strength data came from 11 tests from another project with HF-1 steel. The best curve fit was with a double-exponential distribution with a 93% goodness-of-fit. The average value was 1108-MPa and the standard deviation was 19.4-MPa. The ultimate

Table 1
Measured yield strengths, 12 heat treated lots, HF-1 steel.

Lot	Projectile body sample							
	High hardness body				Low hardness body			
	Area A		Area B		Area A		Area B	
	Yield (MPa)	Elong. %	Yield (MPa)	Elong. %	Yield (MPa)	Elong. %	Yield (MPa)	Elong. %
L5486	755	14.6	735	13.7	682	14.8	672	13.8
7713	748	12.7	685	11.2	643	15.9	647	15.9
L6250	683	11.7	688	12.8	676	13.2	664	12.3
9470	811	12.9	710	13.0	561	18.4	669	15.7
W1083	724	12.3	713	14.6	734	9.6	763	10.7
W2379	747	10.3	754	13.1	650	13.4	638	14.1
W2983	716	10.7	776	11.3	651	11.1	643	13.7
W5823	699	10.7	726	11.6	666	11.6	639	11.1
W6921	780	9.5	746	10.0	635	16.0	625	13.0
Y0640	877	15.0	870	15.0	842	15.0	856	12.0
Y2761	725	11.0	718	11.0	670	9.5	656	10.0
Y6017	718	10.0	780	12.0	611	13.0	646	12.0
Mean	749	11.8	742	12.4	669	13.5	676	12.9
Max	877	15.0	870	15.0	842	18.4	856	15.9
Min	683	9.5	685	10.0	561	9.5	625	10.0
Stdev	53	1.8	51	1.5	69	2.7	67	1.9

Table 2
Reject rate per inspection lot.

| Part #12991157 wall thickness inspection summary | | | | |
| Lot | Quantity | Thin wall | | Rate (%) |
		Accepted	Rejected	
33	3600	3584	16	0.44
33	1800	1792	8	0.44
33	2025	2015	10	0.49
33	150	150	0	0.00
33	400	400	0	0.00
34	1350	1350	0	0.00
34	5050	5047	3	0.06
34	2325	2324	1	0.04
32	3000	2995	5	0.17
6	1400	1393	7	0.50
6	2025	2022	3	0.15
6	3600	3592	8	0.22
6	1200	1200	0	0.00
6	1425	1424	1	0.07

tensile strength in Ref. [13] was reported to be 1195 ± 18 MPa, similar to the empirical data.

3.3. Defect functions

Out of the first 24,300 bodies that were manually gaged, 59 anomalies were in non-conformance to the wall thickness, Fig. 4. The variation in conforming wall thickness was not recorded. The effect of anomaly depth was included in the stress and strain calculations and not used as a separate distribution in the probability estimate.

In a study of 14 lots of mortar projectile, the rate of defects varied between 0.0 and 0.005025. Several lots had zero defects. Using DistributionProbe [10], the best curve fit to the data was a uniform distribution between the two defect rates.

3.4. Load function

The forces in a gun tube and statistical variation were measured from actual gun shots. The average and standard deviations for the outside pressure, the *G*-forces, and the fuze load were supplied and used in the analysis. Values are shown in Table 3. For the limit state functions, the load variations were normalized to 1.

3.5. Finite element analysis, stress and strain functions

Finite element analysis was used to find the stresses and strains in the limit state functions shown in Eqs. (2) and (3). The general-purposed finite element program ABAQUS Standard [15] was used for analysis. The finite element representation is shown in Fig. 5. Geometry included shells without anomalies and shells with anomalies in the range shown in Fig. 4. Eight-node brick elements were used. The material, HF-1 Steel, was modeled as elastic–plastic. Analyses were run with the yield strength and elongation specified on the drawing.

Several load cases were reviewed. An initial proof load of 63.8 MPa was applied to the inside of the shell. Later steps applied a pressure load to the outside of the shell, a fuze load, and *G*-forces, Table 3. The external pressure was applied rearward of the obturator, as indicated in Fig. 5. The fuze was assumed to be tied to the shell at the forward end of the mortar shell. Other parts attach to the shell limiting motion in the radial direction as indicated in Fig. 5. Analysis was repeated with different flaw depths. For the limit state function, stresses and strains were found using the average load and different geometries.

The stresses and strains shown in Table 4 were used for statistical analysis. The middle line for 0.076 cm is consistent with the minimum conforming wall thickness. The bottom anomaly depth 0.254 cm is consistent with the maximum anomaly found in the screened projectiles, non-conforming. Anomalies larger than the 0.076 cm depth had some yielding at the maximum depth of the flaw. The region of yielding circumferentially was local to the defect and not considered a failure condition [12].

3.6. Boundary condition function

There is some uncertainty associated with boundary conditions in a finite element analysis. Fig. 5 shows a quarter model of the mortar body. At one end of the mortar, to the left in the picture, other components attach to the mortar. It is not clear how
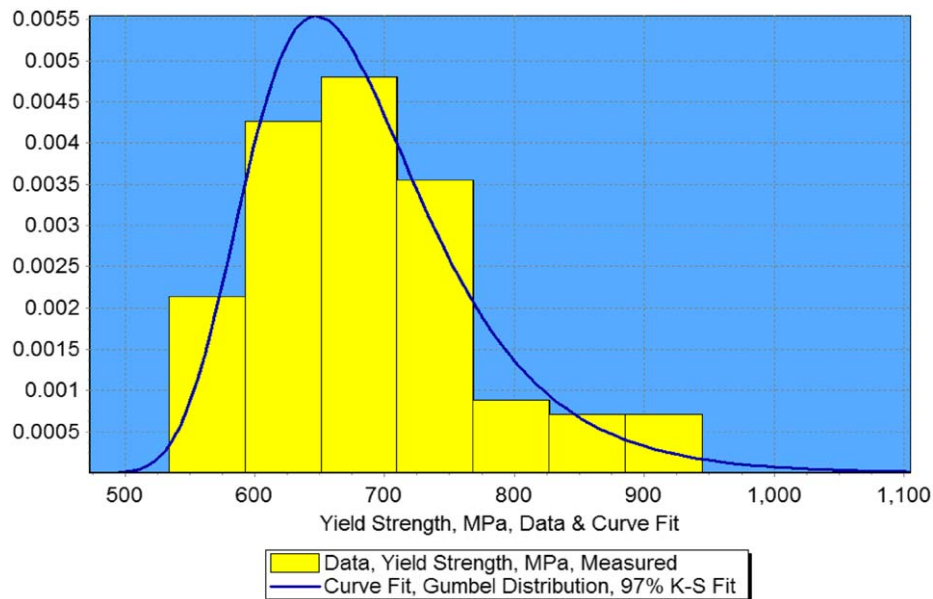
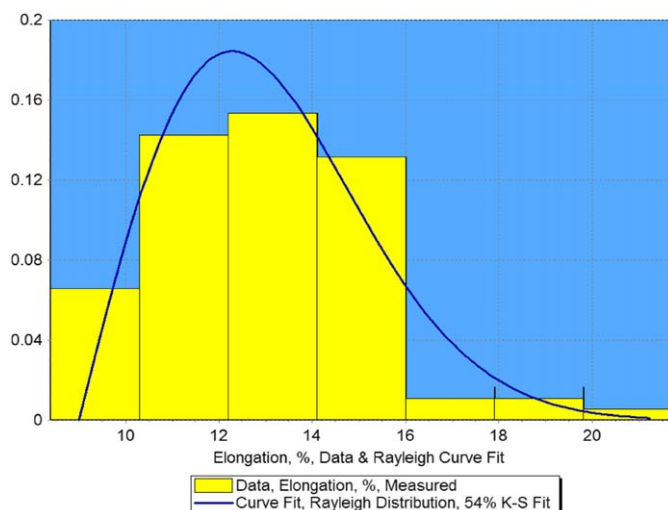**Fig. 2.** Curve fit of measured yield strength data.

Fig. 3. Curve fit of measured elongation data.

much constraint these other components represent. Similarly, at the forward end of the mortar, a fuze is applied. At both ends, the amount of constraint and contact is unknown and probably varies from mortar to mortar. To account for that uncertainty, finite element models were done with different levels of constraint at either end of the mortar shell. The difference in maximum stress at the flaw for different boundary assumptions was 13.6%. This variation was included in the analysis as an uncertainty in the stress and strain.

3.7. Data summary

Table 5 summarizes the probability distributions used for analysis. Stresses and strains retained the MPa units. Other uncertainties were normalized to 1. The functions $F1$–$F9$ relate to the functions discussed in Section 4.

4. Results

4.1. Limit state functions

A number of limit state functions were used to check the probability of a failure. The basic form of the limit state functions is shown in Eqs. (1) and (2).

4.2. Trial 1—estimate of yield failure

Yielding is not a safety-critical failure but was checked at the customer request. Eq. (3) was used to estimate yielding:

$$G1a = Sy - F1 \times F2 \times F3(1 - F4) - F5 \times F6 \times F7 \times F8 \qquad (3)$$

- Sy = yield function, from experimental data, maximum Gumbel, Fig. 2, average = 685 MPa, standard deviation = 84.6 MPa.
- $F1$ = stress distribution, assumed uniformly distributed in the range [332–526], maximum von Mises stress for zero flaw and minimum allowable wall thickness, from the finite element method, Table 4.
- $F2$, $F6$ = normalized load function, from experimental data, lognormal distribution, average = 1, COV = 0.042, from Table 3.
- $F3$, $F7$ = finite element constraint, assumed lognormal distribution, average = 1, COV = 0.136, from finite element analysis with different constraint assumptions.
- $F4$, $F8$ = quantity of anomalies, 14 measured lots, curve fit to uniform distribution, between [0–0.005025], Table 2.
- $F5$ = stress, assumed uniformly distributed in the range [526–739], maximum von Mises stress for minimum allowable wall thickness and minimum wall thickness as measured, Fig. 4.

Three probability methods were compared: Monte Carlo Simulation, 1st-, and 2nd-order approximations. Probability of yielding was estimated at 1.3%, 1.9%, and 1.4%, respectively using the three methods. The 1st- and 2nd-order estimates provided reasonable results with fewer than 100 trials. Since yielding would not cause a safety-critical failure, strength results were repeated with ultimate tensile strength.
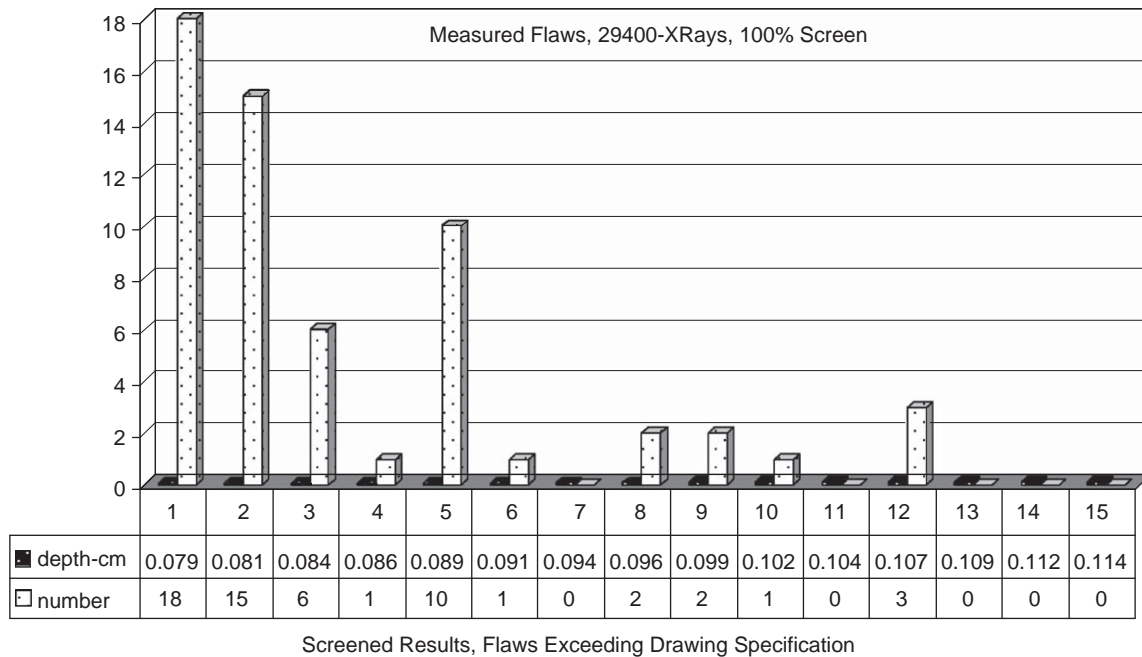
Fig. 4. Distribution of measured anomaly depths.

Table 3
Load on mortar shells.

Name	Outside pressure (MPa)	G-force	Fuze (kg)
Load−3σ	46.3	7393	478.2
Load	53.2	8483	478.2
Load+3σ	60	9574	478.2

4.2. Trial 2—probability of exceeding tensile strength

Stress exceeding ultimate tensile strength could result in a safety-critical failure. If the likelihood of a safety-critical failure exceeds 1/1E6, the mortars could not be used. The limit function shown in Eq. (3) was altered to compare stresses to ultimate tensile strength:

$$G1b = \text{Sult} - F1 \times F2 \times F3(1 - F4) - F5 \times F6 \times F7 \times F8 \qquad (4)$$

Sult is the ultimate tensile strength function, from US Army metallurgist at Picatinny Arsenal, curve fit of 11 data points, double exponent, average = 1120 MPa, standard deviation = 19.6 MPa

The other functions were the same as used for yield strength. With the 1st-order method, the estimated probability of failure was 4.5E−9, less than 1 in a million as required. The Monte Carlo simulation provided 0 failures in 10E6 trials.

4.3. Trial 3—probability of exceeding material elongation

If the strain exceeds the material elongation, a safety-critical failure could result. The limit function shown in Eq. (5) was used to assess the likelihood of strain exceeding the material elongation:

$$G2 = e1 - F9 \times F2 \times F3(1 - F4) - F10 \times F6 \times F7 \times F8 \qquad (5)$$

- Elongation = $e1$ = Measured experimentally and curve fit, Rayleigh distribution, mean 0.13 and standard deviation 0.02, Fig. 3.
- $F9$ = strain distribution, assumed uniformly distributed in the range [9.3E−4–1.03E−3], maximum von Mises strain for no flaw and for the minimum allowable wall thickness.

- $F10$ = strain distribution, assumed uniformly distributed in the range [1.03E−3–2.4E−3], maximum von Mises strain with minimum conforming wall thickness and maximum non-conforming measured wall thickness, Fig. 1 and Table 4.

The other functions were the same as used for yield strength. No failure points were found in 10E6 Monte Carlo simulations. The 1st- and 2nd-order methods gave a warning, presumably indicating no failure condition.

5. Discussion

5.1. Traditional approach, finite element results

For comparison, mortar shell was also evaluated using traditional methods at the margin overload. Gun-launch projectiles are traditionally evaluated with the PMP+5% condition [12,16]. PMP +5% refers to 105% of the permissible maximum pressure in a weapon as defined in International Test Operating Procedure (ITOP) 4-2-504. PMP coincides with a 3-sigma upper limit on the service charge conditioned to +145 °F. Statistically, PMP load occurs 13 in 10,000 firings and PMP +5% occurs slightly under 1 in a million firings [12,16].

The PMP+5% loads were applied to the finite element model based on the geometry in Fig. 1. The maximum stress was 811 MPa, less than the ultimate tensile strength and acceptable. The maximum plastic strain, 0.03 cm/cm, was less than material elongation and acceptable. The maximum yield through the wall ligament was about 3/4 of the thickness at the flaw. The region was circumferentially local and acceptable. The load to plastically collapse the mortar body with a 0.254-cm-flaw was 1.7 × PMP+5% load, acceptable. Load to elastically collapse a mortar body with the 0.1-cm-flaw was 7.6 × PMP+5%, acceptable. Based on deterministic analysis, the mortar body with a 0.254-cm-flaw has adequate margin against a safety-critical failure.

As a check on the critical anomaly depth on the drawing, the critical anomaly depth was estimated for proof test. The software package NASGRO [17] and the methods described in Ref. [12] were used to estimate the critical anomaly depth. The range of fracture
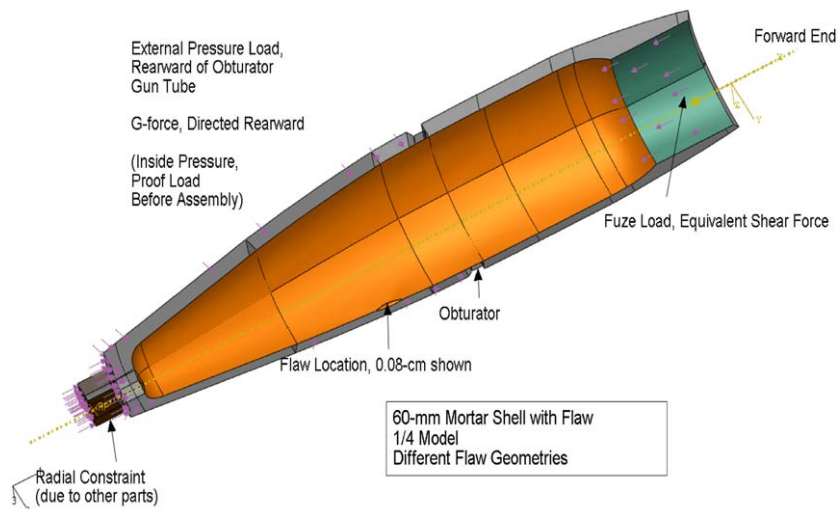
Fig. 5. Finite element representation.

Table 4
Finite element results, stress and strain.

Flaw depth (cm)	von Mises stress at anomaly Average load (MPa)	Strain at anomaly (cm/cm)
0	332.4	9.34E−04
0.076	526.2	1.03E−03
0.254	739.5	2.39E−03

Table 5
Summary of variables.

Variable	Variable	Distribution	Parameters	Source of data
Yield strength	S_y	Maximum Gumbel	Average = 685 MPa; Standard deviation = 84.6	Experimental yield strengths, DistributionProbe curve fit, Table 1
Maximum stress at flaw, geometry conforming	$F1$	Uniform	Minimum = 332 MPa; Maximum = 526 MPa	Finite element analysis of geometry with no flaw and largest allowable flaw
Normalized load function	$F2, F6$	Lognormal	Average = 1; COV = 0.042	Experimental values from numerous mortar tests, Table 3
Finite element constraint uncertainty	$F3, F7$	Lognormal	Average = 1; COV = 0.136	From finite element analysis, different stresses for different constraint assumptions
Quantity of flaws exceeding specification	$F4, F8$	Uniform	Minimum = 0, Maximum = 0.005025	From 100% measurement of flaws in many lots of mortars, DistributionProbe curve fit, Table 2.
Maximum stress at flaw, geometry not conforming	$F5$	Uniform	Minimum = 526 MPa; Maximum = 739 MPa	Finite element of analysis of geometry with largest allowable flaw and largest measured flaw from 100% screening, Table 4
Ultimate Tensile Strength	S_{ult}	Double exponent	Average = 1120 MPa; Standard deviation = 19.6 MPa	Experimental tensile strength, DistributionProbe curve fit
Elongation	$E1$	Rayleigh	Mean = 0.013; standard deviation = 0.02	Experimental elongations, DistribibutionProbe curve fit, Fig. 3
Maximum strain at flaw, geometry conforming	$F9$	Uniform	Minimum = 9.3E−4 mm/mm; Maximum = 1.03E 3 mm/mm	Finite element analysis of geometry with no flaw and largest allowable flaw
Maximum strain at flaw, geometry not conforming	$F10$	Uniform	Minimum = 1.03E 3 mm/mm; Maximum = 2.4E 3 mm/mm	Finite element of analysis of geometry with largest allowable flaw and largest measured flaw from 100% screening, Table 4

toughness was given by an Army metallurgist between 24.7 and 37 MPa√m. The critical anomaly depth was in the range shown in Fig. 1. The estimated critical anomaly depth was slightly larger indicated by the allowable wall thickness range. Changes were not recommended.

5.2. Comparison of traditional and statistical analyses

A traditional analysis at the PMP+5% gun load predicted that a safety-critical failure would not occur. The statistical method provided a numerical estimate of the number of failures in one million firings. Results were consistent. Mortar projectiles were acceptable for release.

5.3. Process improvements

As a result of the anomalies, several additional actions were taken:

1. All 60-mm projectile bodies are now 100% screen for non-conforming parts. The wall thickness inspection method has also been improved by replacing the manual gaging with an automated 100% ultrasound wall thickness inspection.

2. The production process was changed to include machining of the entire interior cavity of the projectile body after forging.

6. Conclusions

Statistical analyses were done to determine the probability of a safety-critical failure of mortar shells. Several variations were included in the study. While yielding is predicted to occur in about 2% of the shells, the probability of a safety-critical failure is much less than 1 in a million, as required. The mortars have all been released and used in Iraq and Afghanistan. No safety-critical failures were reported, consistent with the statistical predictions and traditional calculations.

Acknowledgments

References

[1] Heitzer M, Staat M. Reliability analysis of elasto-plastic structures under variable loads. In: Weichert D, Maier G, editors. Inelastic analysis of structures under variable loads: theory and engineering applications. Dordrecht: Kluwer Academic Press; 2000. p. 269–88.

[2] Gumbert CR, Hou GJ-W, Newman PA. Reliability assessment of a robust design under uncertainty for a 3-D flexible wing. In: 16th AIAA computational fluid dynamics conference, Orlando, FL, 2003.

[3] Gumbert CR, Newman PA, Hou GJ-W. Effect of random geometric uncertainty on the computational design of a 3-D flexible wing. In: 20th AIAA applied aerodynamics conference, St. Louis, MO, 2002.

[4] Gumbert CR, Hou GJ-W, Newman PA. Simultaneous Aerodynamic and Structural Design Optimization (SASDO) of a 3-D wing. In: 15th AIAA computational fluid dynamics conference, Anaheim, CA, 2001.

[5] Putko MM, Newman PA, Taylor II, AC, Green LL. Approach for uncertainty propagation and robust design in CFD using sensitivity derivatives. In: 15th AIAA Computational Fluid Dynamics Conference, Anaheim, CA, 2001.

[6] Shah AR, Korovaichuk I. Stirling convertor fasteners reliability quantification. NASA/TM—2006-213992, 2006.

[7] Moglia M, Davis P, Burn S. Strong exploration of a cast iron pipe failure model. Reliability Engineering & System Safety 2008;93:885–96.

[8] Recchia S, Cordes JA, Kahlessi MR, Worthington M. Improving reliability by reducing tolerance stack-up failures. Technical report ADA443508, ARDEC, Picatinny Arsenal, NJ & DTIC report ARAET-TR-05018, 2005.

[9] Reinhardt L, Cordes JA, Geissler D, Strickland K, Walter WS. Improving the reliability of a self-destruct fuze using dynamic structural analysis. Technical report ARMET-TR-08011, ARDEC, Picatinny Arsenal, NJ, October, 2008.

[10] Unipass, Version 5.9. PredictionProbe Inc., Irvine, CA, USA, 2007.

[11] DistributionProbe, V1.2. PredictionProbe Inc., Irvine, CA, USA, 2006.

[12] Cordes JA, Carlucci DE, Kalinowski J, Reinhardt L. Design and development of reliable gun-fired structures. Technical report AD no.: ADA455406 Army Armament Research Development and Engineering Center Picatinny Arsenal, NJ, Technical Research Center, 2006.

[13] Saunders DS. Mechanical properties and fracture toughness assessment of M795 and M549 155 MM artillery projectile bodies manufactured from HF-1 steel, Report MLR-R-1007, DTIC AD-A174813, 1986.

[14] Metallic Materials Properties Development and Standardization (MMPDS), Department Of Transportation report DOT/FAA/AR-MMPDS-01, January 2003.

[15] ABAQUS Standard, Version 6.5.6. Dassualt Systems Simulia Corp., Providence, RI, 2006.

[16] Safety Testing of Fuzed Artillery Ammunitions. International Test Operations Procedure 4-2-504(1). 1993. Ad no. A274371.

[17] NASGRO 5.0. Southwest Research Institute, San Antonio, TX, 2006.